The initiation and early development of the tubulin-containing cytoskeleton in the human parasite *Toxoplasma gondii*

Luisa F. Arias Padilla, John M. Murray, and Ke Hu*

Biodesign Center for Mechanisms of Evolution/School of Life Sciences, Arizona State University

ABSTRACT The tubulin-containing cytoskeleton of the human parasite *Toxoplasma gondii* includes several distinct structures: the conoid, formed of 14 ribbon-like tubulin polymers, and the array of 22 cortical microtubules (MTs) rooted in the apical polar ring. Here we analyze the structure of developing daughter parasites using both 3D-SIM and expansion microscopy. Cortical MTs and the conoid start to develop almost simultaneously, but from distinct precursors near the centrioles. Cortical MTs are initiated in a fixed sequence, starting around the periphery of a short arc that extends to become a complete circle. The conoid also develops from an open arc into a full circle, with a fixed spatial relationship to the centrioles. The patterning of the MT array starts from a "blueprint" with ~five-fold symmetry, switching to 22-fold rotational symmetry in the final product, revealing a major structural rearrangement during daughter growth. The number of MT is essentially invariant in the wild-type array, but is perturbed by the loss of some structural components of the apical polar ring. This study provides insights into the development of tubulin-containing structures that diverge from conventional models, insights that are critical for understanding the evolutionary paths leading to construction and divergence of cytoskeletal frameworks.

Monitoring Editor Xueliang Zhu Chinese Academy of Sciences

Received: Nov 3, 2023 Revised: Dec 11, 2023 Accepted: Dec 19, 2023

SIGNIFICANCE STATEMENT

- The tubulin-containing cytoskeleton of the human parasite *Toxoplasma gondii* includes several distinct structures. How they are assembled in nascent daughter parasites is poorly understood.
- Using 3D-SIM and expansion microscopy, we found that assembly of the cortical microtubules and conoid initiate almost simultaneously in close proximity and both proceed towards the centrioles. After nucleation is completed, the microtubule array adopts ~five-fold symmetry, subsequently switching to 22-fold rotational symmetry.
- This study provides insights into the development of tubulin-containing structures that diverge from conventional models, insights that are critical for understanding the evolutionary paths leading to construction and divergence of cytoskeletal frameworks.

This article was published online ahead of print in MBoC in Press (http://www .molbiolcell.org/cgi/doi/10.1091/mbc.E23-11-0418) on January 3, 2024. Conflict of Interest Statement: The authors declare that they have no conflict of

*Address correspondence to: Ke Hu (kehu4@asu.edu).

Abbreviations used: SIM, structured illumination microscopy; ExM, expansion microscopy; MT, microtubules; CCS, cosmic calf serum.

© 2024 Padilla et al. This article is distributed by The American Society for Cell Biology under license from the author(s). Two months after publication it is available to the public under an Attribution–Noncommercial–Share Alike 4.0 Unported Creative Commons License (http://creativecommons.org/licenses/by-nc-sa/4.0).

"ASCB®," "The American Society for Cell Biology®," and "Molecular Biology of the Cell®" are registered trademarks of The American Society for Cell Biology.

INTRODUCTION

The cytoskeleton provides the structural basis underlying cell shape and mechanical stability, as well as various intracellular activities such as vesicular transport and force generation. The characteristic cytoskeletal arrangement in different cell types is coupled with specific cellular function and activities. Among the thousands of species of apicomplexan parasites, one of the shared characteristic cytoskeletal architectures is the set of cortex-associating (variously denoted as "subpellicular" or "cortical") microtubules (MTs; Figure 1). The number of MTs and their arrangement within the array is species-specific, and highly reproducible within each species

(Garnham et al., 1962; Bannister and Mitchell, 1995; Morrissette and Sibley, 2002a; Bounkeua et al., 2010; Wang et al., 2020). Apicomplexans are responsible for many high-impact and often devastating diseases, including malaria, cryptosporidiosis, and toxoplasmosis (Torgerson and Mastroiacovo, 2013; Checkley et al., 2015; Seeber and Steinfelder, 2016; World-Health-Organization, 2022). Their tubulin-containing cytoskeleton provides a potential rich source of drug targets (Morrissette, 2015). In Toxoplasma gondii, a prototypical apicomplexan, the cortical MTs are stabilized by a suite of novel associated proteins (Tran et al., 2012; Liu et al., 2013, 2015; Leung et al., 2017). Chemical inhibition of the elongation of the cortical MTs during cell division results in a distorted cortex and nonviable progeny (Stokkermans et al., 1996; Morrissette and Sibley, 2002b; Fennell et al., 2006; Hu et al., 2006; Hu, 2008). In addition, unlike most polarized microtubule arrays examined so far, which typically originate from a centrosome or spindle pole, the cortical MTs of Toxoplasma and other apicomplexans are anchored in the apical polar ring, an annular structure at the parasite apex (Nichols and Chiappino, 1987; Bannister and Mitchell, 1995; Morrissette et al., 1997; Morrissette and Sibley, 2002a; Leung et al., 2017). Genetic manipulations that disrupt the integrity of the apical polar ring result in abnormalities in the MT array, failed mosquito transmission for Plasmodium ookinete (Qian et al., 2022) and highly impaired lytic cycle for the Toxoplasma tachyzoite (Leung et al., 2017; Tosetti et al., 2020; Back et al., 2021). In Toxoplasma, the same tubulin subunits that polymerize into the cortical MTs are also the building blocks for the conoid, which is formed of 14 ribbonlike, novel tubulin polymers organized into a left-handed spiral (Hu et al., 2002b; Sun et al., 2022; Gui et al., 2023; Li et al., 2023; Figure 1). Like a piston, the conoid can protrude and retract in a calcium-dependent manner, passing through the apical polar ring (Hu et al., 2002b, 2006). The disruption of the conoid structure severely impairs parasite invasion into the host cell (Nagayasu et al., 2016; Long et al., 2017; Back et al., 2020; Tosetti et al., 2020; Dos Santos Pacheco et al., 2021; O'Shaughnessy et al., 2023).

The apicomplexans use a "born-within" mode of cell division (endodyogeny, endopolygeny, or schizogony). During cell division, the daughter cytoskeleton is built from scratch instead of rearranged from the preexisting maternal cytoskeleton, which allows immediate and unambiguous recognition of the daughter cytoskeletons underconstruction versus the fully established maternal structure (Hepler et al., 1966; Sheffield and Melton, 1968; Sheffield, 1970; Dubremetz and Elsner, 1979; Hu et al., 2002a; Morrissette and Sibley, 2002a; Voß et al., 2023). The coexistence of mature (i.e., mother) as well as forming (i.e., daughter) cytoskeletons also provides a convenient model to address how distinct biochemical states of apparently identical cellular structures can exist in the same cell within rapid diffusion distance from each other, and how one state can develop into the other (Liu et al., 2015; Tengganu et al., 2023). Together, the stunning reproducibility, ordered arrangement, and readily observed de novo construction of the tubulin-containing cytoskeleton in apicomplexans enable the discovery of structural features and transitions difficult to detect in other less well-ordered systems. It is therefore a superior model for determining the structural basis for constructing a defined cytoskeletal framework.

The *T. gondii* tachyzoite has 22 spirally arranged cortical MTs (Figure 1). In mature parasites, these MTs form an ultrastable "rib cage" and remain intact indefinitely (in experimental terms) under treatments that depolymerize MTs in mammalian cells within minutes (Morrissette *et al.*, 1997; Hu *et al.*, 2002b). When three associated proteins are all removed, the cortical MTs in mature parasites are destabilized, which results in surprisingly little change in parasite

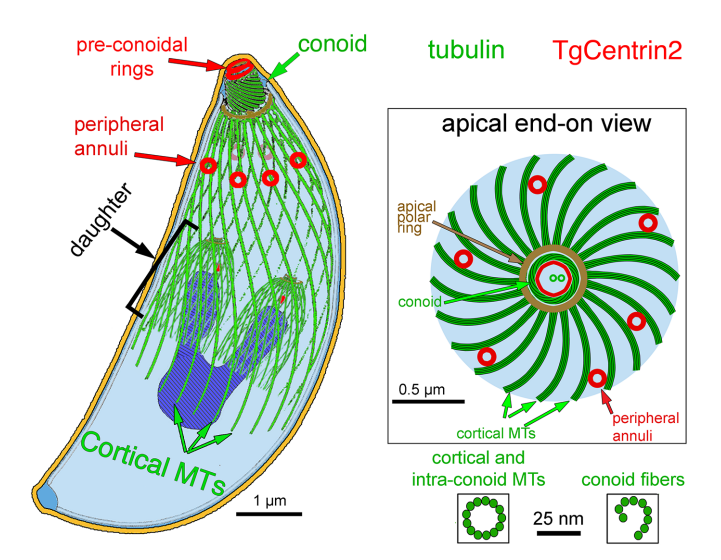


FIGURE 1: Cartoon drawings of T. gondii viewed from the side (left) and end-on from the apical end (right). Tubulin-containing structures are green, TgCentrin2-containing structures are red. In the side view, the preconoidal rings are shown atop the conoid, and centrin2containing annuli are distributed around the periphery. The conoid fibers are ribbon-like tubulin polymers with a protofilament arrangement very different from that in a microtubule (cross sections shown on the lower right side). The plasma membrane is shown in orange, and the apical polar ring in brown. Inside the mature parasite, the developing cortical microtubule arrays that envelop two midstage daughters are shown. The nucleus (dark blue) is shown being partitioned between the daughters. Within the daughters, a red dot indicates the location of the centrin2-containing centrioles. For clarity, other organelles are not shown. Viewed from the apical end, the 22 cortical MTs are shown anchored in the apical polar ring, which encircles the conoid. The two intra-conoid MTs (green) are seen through the preconoidal rings (red).

shape, but in a dramatic change from helical to linear parasite movement in a three-dimensional matrix (Liu et al., 2015; Tengganu et al., 2023). The roots of the cortical MTs are located at evenly spaced intervals around the circumference of the apical polar ring, separated by cogwheel-like projections (Nichols and Chiappino, 1987; Morrissette et al., 1997; Morrissette and Sibley, 2002a; Leung et al., 2017). Although it does not contain γ-tubulin (Morrissette, 2015; Suvorova et al., 2015), the apical polar ring is likely to be the organizing center for the cortical MTs. We previously showed that the cortical MTs grow at their distal ends (Hu et al., 2002b), suggesting that their minus ends are anchored at the apical polar ring as proposed earlier (Russell and Burns, 1984). This polarity arrangement was later confirmed by cryo-electron microscopy studies (Wang et al., 2021; Sun et al., 2022; Li et al., 2023). During cell division, while the mitotic spindle is assembled in the nucleus, the cortical MTs of the developing daughter polymerize in the cytosol (Liu et al., 2015). Simultaneously the conoid also develops in close proximity to the apical ends of the cortical MTs (Hu et al., 2006; Hu, 2008).

While much progress has been made in the structural analysis of the cytoskeleton of mature parasites (Morrissette et al., 1997; Hu et al., 2002b, 2006; Wang et al., 2021; Sun et al., 2022; Gui et al., 2023; Li et al., 2023), knowledge of the initial stages of daughter development is lacking. For example, is there a defined pattern in the initial assembly process? Are all 22 cortical MTs nucleated at the same time or sequentially? Are the cytoplasmic tubulin-containing structures-the cortical MTs, conoid, and intra-conoid MTs- nucleated from the same or distinct precursor structures? Answering these

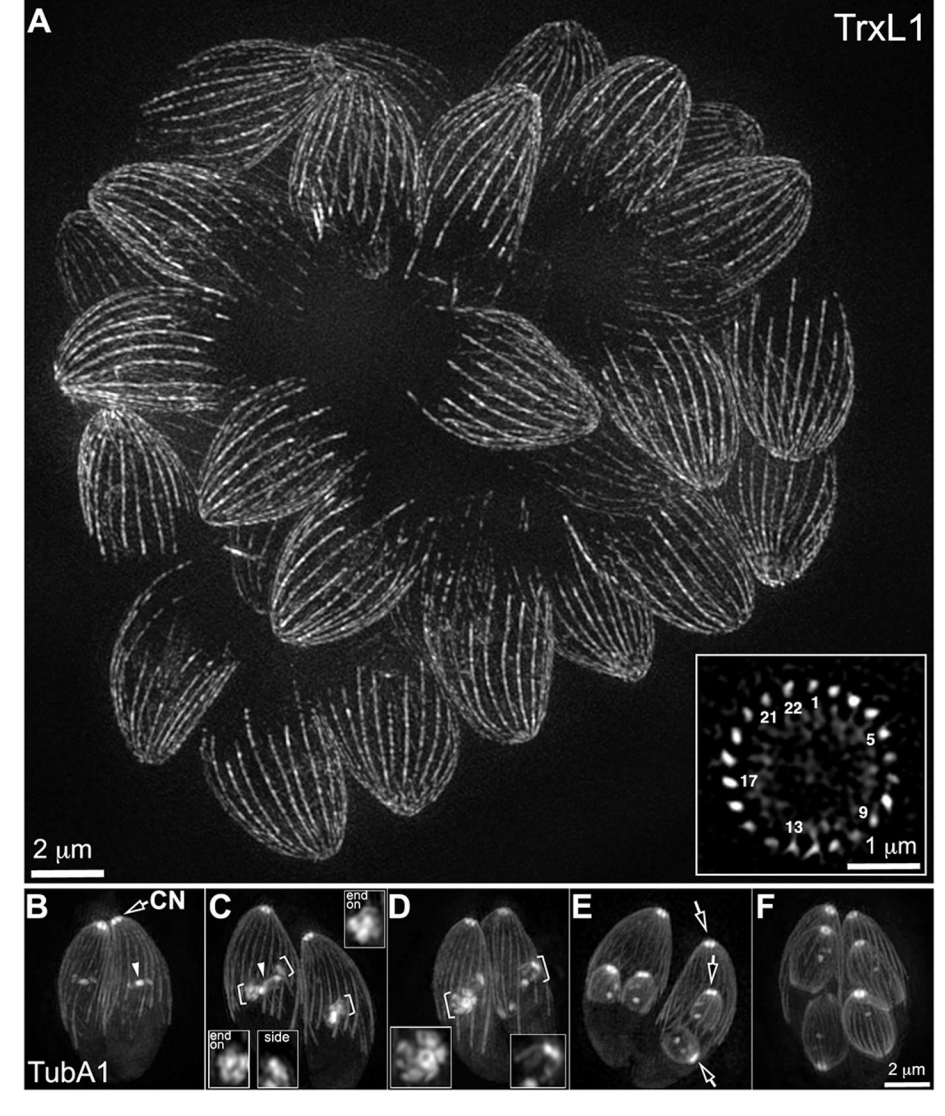


FIGURE 2: The cortical MT array switches from approximate five-fold to 22-fold rotational symmetry during development. (A) Projections of 3D-SIM images of live Toxoplasma parasites expressing mEmeraldFP-TrxL1 (Liu et al., 2013), in which cortical MTs are fluorescently labeled. Inset: an end-on view of an optical section through the middle of an adult parasite showing the even distribution of the 22 cortical MTs around the cortex. A subset of the MTs are labeled with numbers. (B-F) Projections of 3D-SIM images of several live Toxoplasma parasites expressing eGFP-lpha1-tubulin at different stages of cell division. Insets (2X, contrast enhanced) include end-on or side views of the nascent daughters indicated by brackets. Image contrast was adjusted to enable better visualization of structures with weaker fluorescence (e.g., cortical MTs) without oversaturating the brighter regions (e.g., conoid labeling). Arrowheads: spindles. Arrows: conoid (CN).

questions will provide important insights into how complex supramolecular assemblies are built with structure that is identical in every cell. Here we use three-dimensional structured illumination microscopy (3D-SIM) and Expansion Microscopy (ExM) to determine the fine structural details of nascent daughters, centered around the construction of the cortical MT array and the conoid.

RESULTS

In the mature parasite, the cortical MTs are evenly distributed around the cortex with ~22-fold rotational symmetry (Figure 2A). To establish the sequence of structural transitions during daughter construction in live parasites, we carried out 3D-SIM imaging of parasites expressing eGFP tagged Toxoplasma α1-tubulin (TUBA1; Figure 2, B-F). Nascent daughters first appear as two disk-like structures (Figure 2C), and then develop into a structure resembling an imperfect five-petaled flower (Figure 2D, also reported in [Liu et al., 2015; Nagayasu et al., 2016; Li et al., 2023]), before elongating and broadening to assume a dome-like shape more similar to that of the mother parasite (Figure 2, E and F). This immediately raises several questions highly relevant to the mechanism of patterning. At the front and center is: how are the cortical MTs arranged in the nascent, disklike array precursor? Also remaining unknown is how the initiation and development of the tubulin-containing fibers of the conoid are related to that of the MT array.

While 3D-SIM imaging of live parasites uncovered some unexpected structural intermediates of the growing cytoskeleton, the resolution in SIM images is insufficient to resolve fine structural details in very early nascent daughters. By expanding biological samples in a hydrogel, ExM has enabled the visualization of structural details much smaller than the resolution limit of conventional light microscopy (Chen et al., 2015; Gambarotto et al., 2019; Wassie et al., 2019; Damstra et al., 2022; Klimas et al., 2023). The ExM method (Gambarotto et al., 2019) has been applied in investigating subcellular details of apicomplexans (reviewed in [Liffner and Absalon, 2023]). Here we use a slightly modified version of this method (see Materials and Methods) to determine the arrangement of tubulin containing structures in developing daughters. Our goal was to determine: 1) the symmetry of the nascent MT array, i.e., whether it has five, 22-fold or other symmetry, and 2) the number of MTs in the array, i.e., whether all 22 MTs are present from the beginning or added incrementally. By comparing the measured diameter of the conoid in SIM images of live parasites with its diameter in ExM images, we determined that the expansion ratio in our experiments varies from ~4.6 to 5.7 fold, with a weighted average of 5.4 fold. This was sufficient to reveal a wealth of structural detail not seen

before in developing daughters. In what follows, all distance measurements made on ExM images are reported after correcting for the experimentally measured gel expansion, i.e., as they would have been measured in images of a live parasite, had that been possible.

Before the appearance of the daughter tubulin cytoskeleton, Toxoplasma centrioles duplicate into two pairs located adjacent to the two poles of the nascent spindle, consistent with previous findings (Hu et al., 2006; Hu, 2008; Francia et al., 2012; Chen and Gubbels, 2013; Francia and Striepen, 2014; Liu et al., 2015; Suvorova et al., 2015). The two centrioles within each pair are clearly resolved in the ExM images. When viewed end on, each centriole can be discerned as a circle (Figure 3A). While the nine singlet MTs

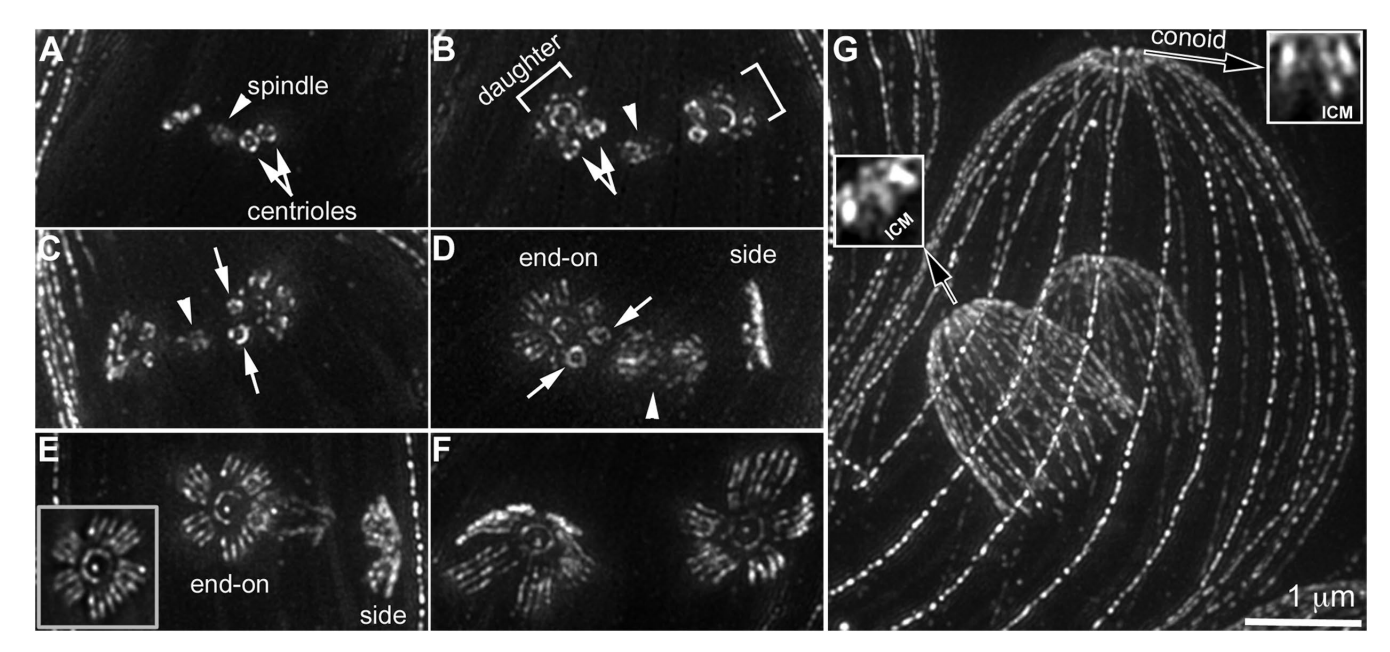


FIGURE 3: Projections of ExM images of wild-type (WT) parasites labeled with an anti-tubulin antibody. Images showing duplicated centrioles adjacent to a forming spindle before the initiation of daughters (A) and pairs of nascent daughters progressing from the initiation to the elongation stage (B–G). The two daughters in the pair in (D and E) are roughly perpendicular to each other, providing end-on and side views. The inset (1X) in (E) is the projection of a subset of the sections showing that all 22 MTs have been nucleated in this daughter. The approximate five-fold rotational symmetry is evident in daughters shown in (F). The cortical MTs are symmetrically distributed in daughters included in G. Insets (2X, contrast enhanced) in (G) include a section through the conoid region of the mother (right) and a daughter parasite (left). ICM: Intra-conoid MTs. Arrowheads: spindle. White arrows: centrioles. Brackets: initiating daughters. Black arrows: conoid. Bars $\approx 1 \ \mu m$ before expansion.

(Morrissette and Sibley, 2002b; Li et al., 2023) are not quite resolved, a substructure with four to five distinct nodes is often seen. The daughter MT arrays first initiate close to the duplicated centrioles (Figure 3, B and C), as six to seven "stubs" of MTs encircling the nascent conoid in a formation that resembles an incomplete smaller version of the "cogwheel" appearance characteristic of the adult apical polar ring as seen in previous EM studies (Leung et al., 2020). This form of structural intermediate was previously unknown and clearly demonstrates that the 22 cortical MTs are not all initiated at the same time. This also indicates that the initial incorporation of nucleation factors or activation of nucleation activity is differentially regulated across/around the MT organizing center. In the disk-like nascent daughters (Figure 3D), individual MTs can be resolved in groups of four and six. The full complement of 22 MTs is unequivocally present when the MTs are only ~0.23 µm long, that is, when there are only ~30 α - β -tubulin heterodimers in each MT protofilament (Figure 3E). Thus, nucleation of the cortical MTs is completed very early during daughter development. At a slightly later stage (Figure 3F), the approximate five-fold symmetry becomes more apparent, with the MTs grouped into "petals" with 4, 4, 4, 4, and 6 MTs, consistent with the five-petal arrangement observed in live parasites by 3D-SIM. To determine the fidelity of the number and organization of MTs in the array, we closely examined 50 very early daughter parasites in which all the cortical MTs could be resolved unambiguously. All fifty of them had 22 MTs. Twenty eight had the grouping pattern of 4, 4, 4, 4, and 6 MTs, and 15 had a pattern that could be easily derived from that grouping (e.g., 4, 4, 6, 2, and 6). Of note, a 4, 4, 4, 4, and 2 grouping was reported in a previous cryo electron-tomography study (Li et al., 2023). We thus propose that the grouping into 4, 4, 4, 4, and 6 MTs is the foundational pattern defined by the location of the nucleation sites.

The number and length of cortical MTs in the array allow one to arrange images of early developing daughters into the correct chronological order (Figure 4). Close examination of the daughter anlagen shows that the conoid codevelops in close proximity to the cortical MT array. The end-on view of the first detectable conoid precursor shows a \sim 0.22 μ m arc (Figure 4A), which is slightly shorter than the expected apparent length of a single conoid fiber tilted as it would be in an adult conoid (\sim 0.36 μ m in length, viewed at \sim 30 degree = 0.31 μ m; Leung et al., 2020). The arc therefore represents only a few, perhaps only one, polymerizing conoid fibers.

The intra-conoid MTs are polymerized slightly after the conoid and cortical MT precursors can be first detected (Figure 4B). In the end-on view, the assembly of the conoid and the cortical MT array always proceed in the same direction, forming arcs with their open side (i.e., the yet-to-be assembled side) oriented towards the centrioles (Figure 4, A–E). The two centrioles are connected by centrin fibers throughout daughter development, with the fibers invariably interacting with the conoid-facing side of the centrioles, as indicated by the labeling with an anti-centrin3 (CEN3) antibody (Figure 4, A–H).

In mature parasites, the conoid fibers are attached to a set of ring-like structures (the preconoidal rings, Figure 1) at their apical ends (Morrissette et al., 1997; Hu et al., 2002b; Sun et al., 2022; Gui et al., 2023). We previously found that another *Toxoplasma* centrin, TgCentrin2 (CEN2), is localized to not only the centriole but also the preconoidal rings, as well as in five to six peripheral annuli (Hu et al., 2006; Leung et al., 2019). Here we examined how these centrin-based structures develop with respect to each other and to the tubulin-containing structures (Figure 4, I–P). We found that similar to CEN3, CEN2 persists at the centrioles throughout daughter development. However, rather than connecting the two centrioles, CEN2

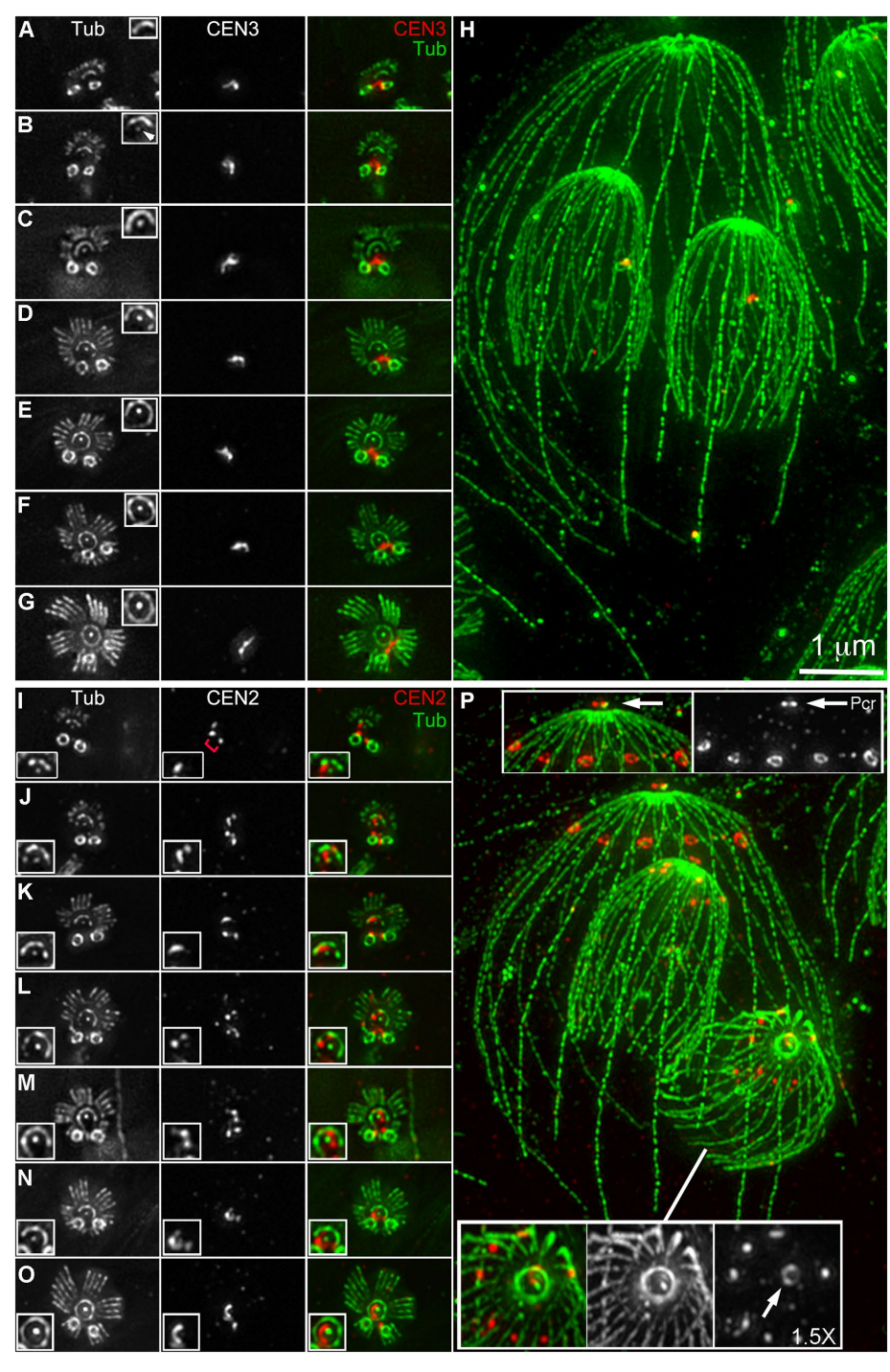


FIGURE 4: The cortical MT array and the conoid in the daughter anlagen grow towards the centrioles. (A-H) Projections of ExM images of WT parasites labeled with an anti-tubulin (gray and green) and an anti-CEN3 antibody (gray and red). (A-G) nascent daughters progressing from initiation to the stage at which the approximate five-fold rotational symmetry has been established. Insets (1.5X, contrast enhanced) include the developing conoid with the intraconoid MTs close to the center (white arrowhead in the inset in B). (H) A dividing parasite in which cortical MTs are symmetrically distributed in daughters. (I-P) Projections of ExM images of WT parasites labeled with an anti-tubulin (gray and green) and an anti-CEN2 antibody (gray and red) with the same arrangement as (A-H). In addition to centrioles, CEN2 highlights the preconoidal rings (Pcr; indicated by arrows in insets in P). The CEN2 signal in the preconoidal rings initially appears as a small focus or a short arc (insets, I-O) adjacent to the intra-conoid MTs. CEN2 also highlights the peripheral annuli (top insets [1X] in P). Note that the peripheral annuli are not detected in early daughters (I-O), but are clearly present in later stage daughters where MTs are more evenly distributed (P, bottom insets, 1.5X, contrast enhanced). Bars ≈ 1 µm before expansion.

often appears as two distinct foci (Figure 41, red bracket). In late daughters or adult parasites, the preconoidal CEN2 is organized into a complete ring (Figure 4P). In nascent daughters, the preconoidal CEN2 signal first appears as a small focus in the immediate neighborhood of the nascent conoid (Figure 4I). Even when the conoid appears to be a complete circle in the end-on view, the preconoidal CEN2 signal is not a ring but an arc, indicating that the preconoidal rings are not yet established at this point (Figure 4O). In view of their tight association with the conoid fibers (Morrissette et al., 1997; Hu et al., 2002b, 2006; Munera Lopez et al., 2022; Sun et al., 2022; Gui et al., 2023), the preconoidal rings might be the organizing center for the conoid. However, this lag between conoid and preconoidal ring maturation seems to argue for some other nucleation sites for conoid fibers.

In adult parasites, the peripheral CEN2 signal is resolved in ExM images as annuli (Figure 4P), consistent with the previous immunoEM analysis (Hu et al., 2006). In daughter parasites, the peripheral CEN2 structures are first detected as spots slightly larger than the point spread function separated by two, four, or six MTs (Figure 4P). These spots appear long after the five-petaled MT array is fully established, indicating that although the CEN2 annuli also display approximate five-fold symmetry, they do not play a role in influencing the structure of the nascent daughter MT array.

The cortical MTs are connected to the apical polar ring, a putative organizing center of the MT array. Previously we discovered that kinesinA and APR1 are two components of the apical polar ring (Leung et al., 2017). The double knockout of the two genes results in the displacement of the cortical MTs from the apex of adult parasites due to the disintegration of the apical polar ring. To determine how and when the structural perturbation of the MT array occurs, we examined the MT structure of daughter parasites of the ΔkinesinAΔapr1 mutant. Upon establishment of the MT petals, 100% (50/50) of the WT daughters have 22 cortical MTs (Figure 5A). However, ~44% (12/27) of daughter parasites in the ∆kinesinA∆apr1 mutant have 23 or 24 MTs (Figure 5B). This indicates that while the nucleating activity per se for cortical MTs is not affected by the removal of kinesinA and APR1, the number of nucleation sites becomes more variable without these scaffold proteins, which affects the fidelity of assembly of the MT array. Aside from the variable number of MTs, the structure of the early daughter MT array in the ΔkinesinAΔapr1

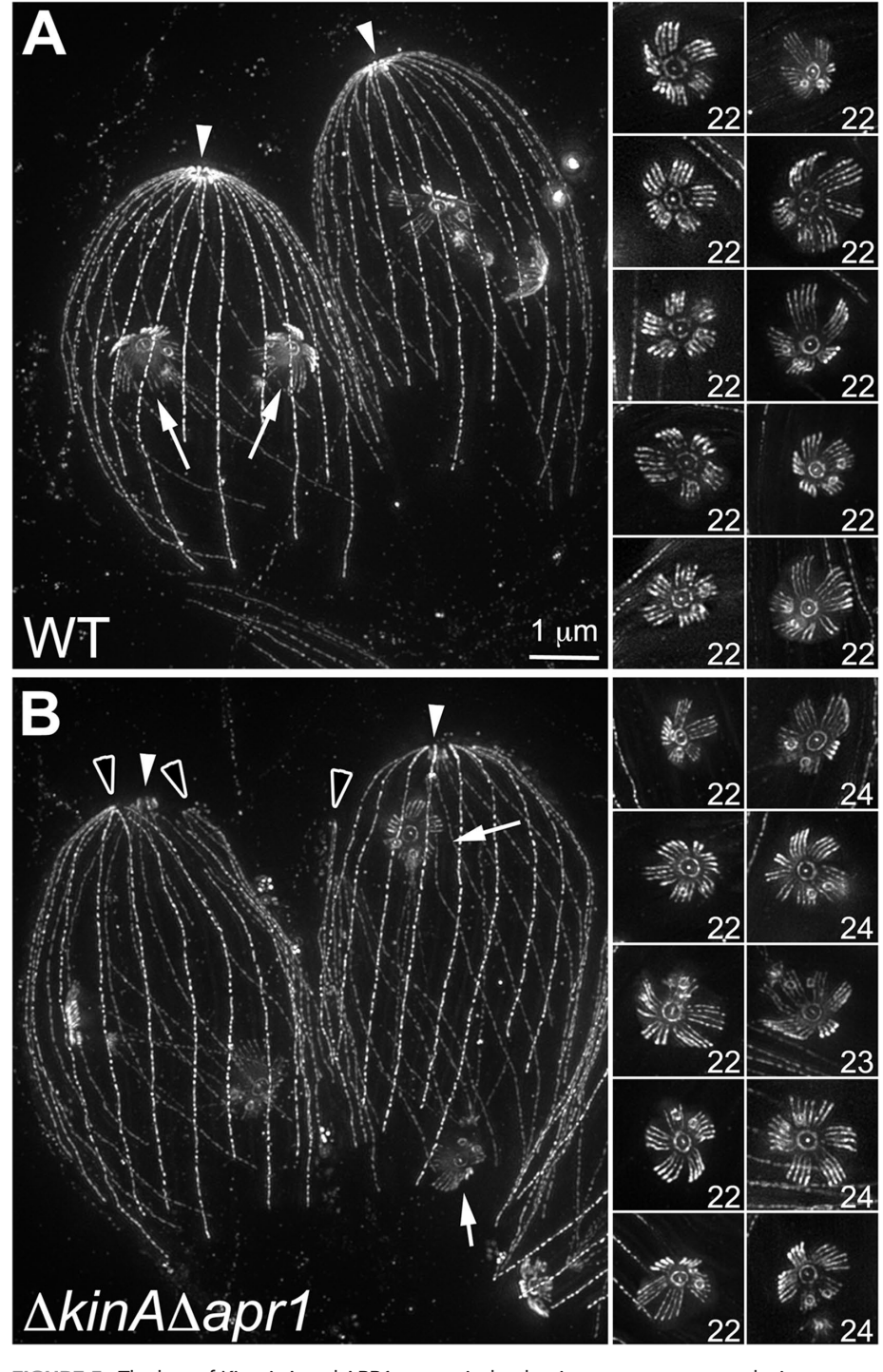


FIGURE 5: The loss of KinesinA and APR1, two apical polar ring components, results in variation in MT numbers in the nascent array. Projections of ExM images of WT (A) and $\Delta kinesinA\Delta apr1$ parasites (B) labeled with an anti-tubulin antibody. A and B include two dividing WT (A) or $\Delta kinesinA\Delta apr1$ (B) parasites with early daughters. Note that clusters of MTs are detached from the apex of the mature $\Delta kinesinA\Delta apr1$ parasites (B, black arrowheads). The right panels include WT (A) or $\Delta kinesinA\Delta apr1$ (B) daughter parasites in which the MT petals are fully established. One of the WT examples (4th row, left column) was also shown in Figure 3F. While the WT parasites always have 22 MTs, the number of MTs in the array in the $\Delta kinesinA\Delta apr1$ parasite varies between 22 and 24. Bars \approx 1 μ m before expansion. Arrows: daughters. White arrowheads: conoid.

mutant appears normal, even though MT detachment is pronounced in the mother parasite (Figures 5B and 6A). This indicates that factors other than or in addition to kinesinA and APR1 are re-

sponsible for MT attachment in early daughter development.

To determine when the detachment of the cortical MTs occur in the $\Delta kinesinA\Delta apr1$ parasites during later daughter development, we measured the incidence of MT detachment in three groups of daughters that have adopted the dome-like shape but with different lengths of MTs. Using the projections of a subset of daughters viewed perpendicular to their long axis, the length of the MTs for the three groups were estimated to be ~1.2 μ m \pm 0.02 (mean \pm SEM, n = 27), 2.0 μ m \pm 0.04 (n = 28), and 3.6 μ m \pm 0.1 (n = 26), respectively. The percentages of daughters with detached MTs were 4.3 \pm 2.6% (mean \pm SEM, n=7 imaging fields, total 70 daughters counted), $18.8 \pm 7\%$ (n = 9 imaging fields, 52 daughters), and $52.1 \pm 4.7\%$ (n = 25 imaging fields, 182 daughters), respectively. Therefore, MT detachment in the daughters becomes more pronounced as daughter MTs elongate in the $\Delta kinesinA\Delta apr1$ parasites (Figure 6, A-C). In contrast, MT detachment was observed in only one out of 160 late-stage (3.0 $\mu m \pm 0.08$, n = 52) WT daughter parasites (Figure 6D). The significant lag in MT detachment after array initiation in the $\Delta kinesinA\Delta apr1$ mutant suggests that the apical polar ring in normal parasites is reinforced as the MT array develops. Previously we discovered that kinesinA is already present in the daughter apical polar ring at the first sign of daughter formation, but APR1 is not detected until later (Leung et al., 2017). Here we examined closely APR1 recruitment to the apical polar ring with respect to daughter growth by measuring APR1mCherry fluorescence and daughter MT length in live APR1-mCherry knock-in parasites expressing GFP-tubulin. We discovered that the level of APR1-mCherry fluorescence is close to background in daughters shorter than ~1 μ m (38 \pm 4, mean \pm SEM, arbitrary units, n = 111 parasites), 130 ± 6 (n = 253) in daughters between ~1–2 μ m, 688 ± 22 (n = 167) in daughters between \sim 3-4 µm, and 1351 \pm 14 (n = 422) for the mother parasite. The Figure 6E and F show SIM imaging of dividing parasites with daughters of different sizes. Note that in the early stage where the MT petals can still be discerned by SIM (Figure 6E, daughter length ~0.66 µm), APR1-mCherry fluorescence is not visible. By the time that APR1 is clearly recruited to the developing daughter apex, the MT petals are no longer well-defined when imaged with 3D-SIM (Figure 6F),

indicating that APR1 recruitment coincides with the symmetry transition of the MT array. We thus propose that the stability of the apical polar ring needs to be strengthened continuously by the recruitment

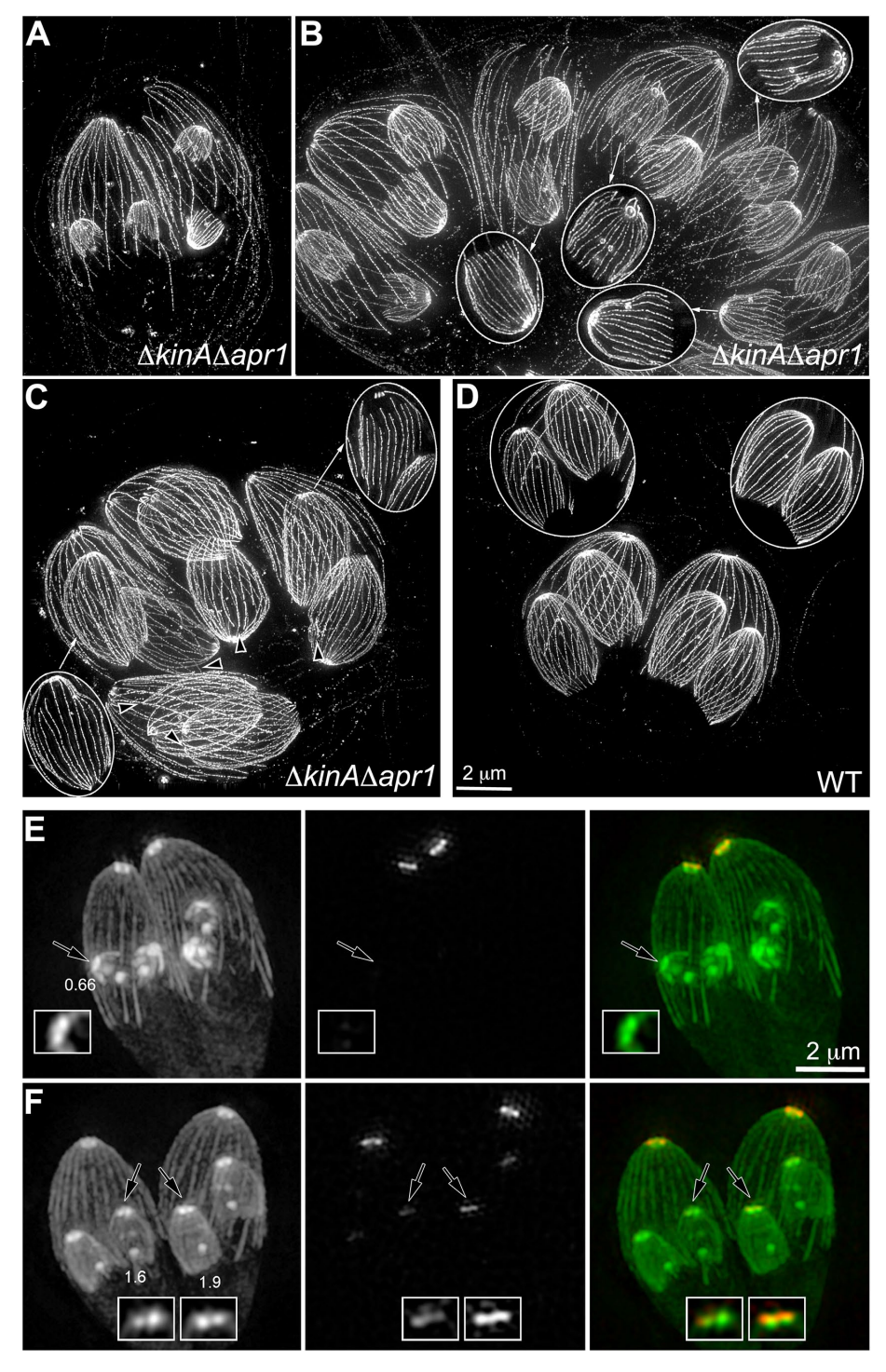


FIGURE 6: Detachment of cortical MTs is detected in ΔkinesinAΔapr1 daughters after the MTs are no longer grouped into petals. (A) Projection of ExM images of $\Delta kinesinA\Delta apr1$ parasites with relatively early daughters. Detachment of the cortical MTs is pronounced in mother parasites, but not observed in daughters. (B) Projection of ExM images of $\Delta kinesinA\Delta apr1$ parasites with daughters in which MT detachment can be detected. Insets (1.3X) include the projections of a subset of the sections to show the detachment of the cortical MTs in four daughter parasites indicated by arrows. (C) Projection of ExM images of ΔkinesinAΔapr1 parasites at a late stage of daughter formation. MTs have detached from the apex in seven out of eight daughter parasites. Insets (1X) include the projections of a subset of the sections to show the detachment of the cortical MTs in two daughter parasites indicated by arrows. Black arrowheads indicate clusters of MT detachment in five other daughter parasites. (D) Projection of ExM images of WT parasites at a late stage of daughter formation. Insets (1X) include the projection of a subset of the sections to show the intactness of the daughter MT array. Bars $\approx 2 \, \mu m$ before expansion.

of the later components (e.g., APR1). This is needed to maintain the integrity of the apical polar ring, possibly to counter tension generated at the MT anchoring sites due to daughter expansion, growth, and changing symmetry of the MT array.

DISCUSSION

The best understood mechanism of the establishment of a polarized MT array comes from studies of animal cells, where the γ tubulin ring complexes embedded in the centrosome matrix serve to initiate and maintain the polarity of the MT cytoskeleton (Oakley and Oakley, 1989; Stearns et al., 1991; Joshi, 1994; Stearns and Kirschner, 1994; Moritz et al., 1995; Patel and Stearns, 2002; Kollman et al., 2008; Oakley et al., 2015). The high concentration of preassembled nucleating complexes at the centrosome provides an intrinsic bias in polarity. In addition, by capping the minus end of the MTs, the effective critical concentration for y-tubulin nucleated MTs is lower than that for uncapped cytoplasmic MTs, further enhancing the preferential MT growth from the centrosome. During mitosis, the interphase array extensively rearranges and reassembles into the biopolar mitotic spindle, but the core principle of the organization of the MT array remains the same (reviewed in [Mitchison, 1988, 1989; Wadsworth, 1993]). Another extensively studied MT-based organelle is the flagellum/cilium, which originates from centrioles (reviewed in [Azimzadeh and Marshall, 2010; Bettencourt-Dias, 2013]).

In the asexual stage of T. gondii, there are five known tubulin-containing structures: the conoid fibers, intra-conoid MTs, cortical MT array, centrioles, and the spindle. During cell division, the spindle is assembled in the nucleus, while the other four tubulin-based structures duplicate (centrioles) or are constructed de novo in the cytoplasm (conoid fibers, intra-conoid MTs, cortical MT array). y-tubulin is found only in the centrosome (Morrissette, 2015; Suvorova et al., 2015),

(E and F) Projections of 3D-SIM images of APR1-mCherry knockin parasites expressing GFP- α 1-tubulin. Note that APR1 is not detected in the apical polar ring of early stage daughters where the MT petals are discernible by SIM (E). Insets (2X, contrast enhanced) include the apex of daughters indicated by arrows. The numbers indicate the length of daughter parasites in µm. Image contrast was adjusted in the tubulin images to enable better visualization of structures with weaker signals (e.g., cortical MTs) without oversaturating the brighter signals (e.g., conoid labeling).

which is likely structurally coupled to the mitotic spindle. Therefore, the construction of the other non-centriole tubulin-containing structures has to involve novel components and perhaps novel mechanisms. Our previous work showed that the conoid and cortical MT array are initiated in the vicinity of the centrioles (Hu *et al.*, 2006; Hu, 2008; Liu *et al.*, 2015), but the resolution was insufficient to discern more structural details.

Here we reveal for the first time the spatial relationship among these structures and how their nascent forms codevelop. Construction of the conoid, intra-conoid MTs, and cortical MTs all begin adjacent to the centrioles with clear structural differentiation in the earliest detectable anlagen (Figures 3 and 4). It is astonishing that three different supramolecular assemblies of quite different structure are being put together from the same pool of tubulin subunits at the same time within a region of ~500 nm across. The assembly of the conoid and the cortical MT array both proceed towards the centrioles, while the intra-conoid MTs grow within the developing conoid slightly after the nascent conoid first appears as an arc in the end-on view. This indicates that these three sets of structures are initiated through distinct but coordinated mechanisms. This opensided intermediate of the conoid is intriguing, because it resembles the architecture of the "pseudoconoid" in the free-living, marine relatives of apicomplexans. The "pseudoconoid" is a half-cone made of a curved sheet of canonical MTs (Portman et al., 2014). The resemblance to the developing conoid is even more suggestive if, as recently proposed, the conoid fibers begin life as canonical MTs (Li et al., 2023) and only later transition to folded ribbons. Many lines of evidence suggest that the ancestor of the apicomplexan parasites descended from a free-living marine protist (Oborník and Lukeš, 2013; Janouškovec et al., 2015; Woo et al., 2015). One thus has to wonder whether the initiation, development, and maturation of the conoid recapitulates how this structure evolved over hundreds of millions of years.

In the nascent daughters, the cortical MTs are already clustered into petals before the nucleation of all 22 MTs is completed. At a later stage, the 22 MTs are organized into a five-petaled structure. In WT parasites, both the organization and the number of MTs are essentially invariant from cell to cell. This basic layout of the array is likely determined by the localization and number of the nucleation sites. In adult parasites, the 22 MTs are not clustered, but instead are evenly distributed around the cortex, that is, arranged with 22-fold rotational symmetry. Therefore, the switch from the approximate five-fold symmetry of the petals to 22-fold symmetry occurs via major rearrangements of MTs rather than addition of new MTs or removal of existing MTs.

Two components of the apical polar ring (kinesinA and APR1) are known to be important for its stability (Leung et al., 2017). The loss of these two proteins destabilizes the apical polar ring, but does not affect the nucleation of the MTs in the cortical array. Interestingly, analysis of early daughter structure in this double-knockout mutant shows however that the fidelity of the MT array is affected. Instead of a constant 22 MTs, a significant number of the double knockout mutant makes 23 or 24 MTs. This suggests that: 1) the nucleating and scaffolding functions of the apical polar ring components are distinct, and 2) the disruption of the scaffold often affects the number of nucleation sites. These observations also highlight the power of the extreme reproducibility of the cytoskeletal structure in *Toxoplasma*, which enables the detection of quite subtle changes in the MT array that would be impossible to detect in most other cell types.

In the adult $\Delta kinesinA\Delta apr1$ parasite, the cortical MTs are dispersed from the apex (Leung et al., 2017). Here we showed that this detachment occurs in the daughter after the initial MT petals have been established. Incidentally, we found the recruitment of APR1 in

WT parasites also accelerates after the initiation stage. This supports the speculation that APR1 reinforces the attachment of the MTs to the developing apical polar ring during the elongation and expansion of the array.

Currently, no nucleation factors have been identified for the cortical MT array, conoid, or the intra-conoid MTs. As these structures are distinct from the centrosome, exploring their nucleation mechanisms will reveal new biology. The structural data reported here can serve as guidance for identifying and interpreting the function of nucleating factors and structural components of the organizing centers.

MATERIALS AND METHODS

T. gondii strains and host cell cultures

Host cell and *T. gondii* tachyzoite parasite cultures were maintained as described previously (Roos et al., 1994; Liu et al., 2015; Leung et al., 2017; Munera Lopez et al., 2022). The Δ kinesin Δ apr1 parasite was reported in (Leung et al., 2017). The mEmeraldFP-TrxL1 knock-in parasite was reported in (Liu et al., 2013). The APR1-mCherry knock-in parasite stably expressing eGFP-Tg α 1-tubulin (TUBA1) was generated by transfecting a ptubA1-eGFP-TgTUBA1 plasmid into the APR1-mCherry knock-in parasite (Leung et al., 2017), selected with 20 μ M chloramphenicol and cloned. The backbone and coding sequence arrangement for ptubA1-eGFP-TgTUBA1 are identical with those for ptubA1-mCherryFP-TgTUBA1 (Leung et al., 2017).

Three-dimensional structured-illumination microscopy (3D-SIM)

Cultures of intracellular parasites growing in human foreskin fibroblast (HFF) cells plated in 3.5-cm glass-bottom dishes (MatTek Corporation, catalogue# P35G-1.5-21-C) were placed in L15 imaging media (Leibovitz's L-15 [21083-027, Life Technologies-Life Technologies, Grand Island, NY] supplemented with 1% [vol/vol] heat-inactivated cosmic calf serum [CCS; SH30087.3; Hyclone, Logan, UT]). Samples were imaged with a DeltaVision OMX Flex imaging station (GE Healthcare-Applied Precision). Image stacks for 3D-SIM were collected at z-increments of 0.125 µm using a 60x oil immersion lens (numerical aperture [NA] 1.42) and immersion oil of refractive index 1.520. Images were reconstructed using Softworx (GE Healthcare-Applied Precision) and the point spread function supplied by the manufacturer. Contrast levels were adjusted to optimize the display.

Sample preparation for ExM

The protocol for ExM basically followed the descriptions in (Gambarotto et al., 2019; Vincent et al., 2022) with slight modifications. Toxoplasma-infected monolayers of HFF cells on 12-mm round coverslips were fixed with 3.6% formaldehyde (made from paraformaldehyde) in phosphate-buffered saline (PBS) for 15-30 min at room temperature, washed several times with PBS, and stored at 4°C in a humidified container. Fixed coverslips were incubated in an anchoring solution (2% acrylamide, 1.4% formaldehyde, in PBS) at 37°C in a humidified chamber for 3-4 hrs. Before gelation, the coverslip with attached cells was incubated with a monomer solution lacking ammonium persulfate (APS) and tetramethylethylenediamine (TEMED; 10% acrylamide, 19% sodium acrylate, 0.1% N,N'-[1,2-dihydroxyethylen]-bisacrylamid [DHEBA]) in the gelation chamber (Vincent et al., 2022) on ice for ~15 min. The monomer solution was then drained. The coverslip was washed briefly with the complete gelation solution (10% acrylamide, 19% sodium acrylate, 0.1% DHEBA, 0.25%TEMED, and 0.25% [wt/vol] APS in PBS) and then incubated with complete gelation solution

in the chamber for 45 min at 37°C. After gelation, the gel with the coverslip was removed from the chamber, placed in a 35-mm dish cell-side up in denaturation buffer (200 mM sodium dodecyl sulfate, 200 mM NaCl, 50 mM TrisCl pH 6.8), and shaken until the coverslip detached from the gel. The gel was then placed in a 2 ml Eppendorf tube with 1 ml of denaturation buffer and incubated for 90 min in a heat block at 84–85°C. The sample was then washed in dH_2O three times before incubation in dH_2O at $4^{\circ}C$ overnight for full expansion. For immunofluorescence labeling, the fully expanded gel was first washed in PBS briefly 3-4 times and equilibrated in PBS for ~30 min to 1 h at room temperature. A small piece of the gel was then removed, placed in a glassbottom dish (MatTek Corporation, catalogue# P35G-1.5-21-C) and incubated with primary antibody at 37°C in a humidified chamber for 3-4 h, washed in PBS + 0.05% tween 20 briefly twice, followed by 15 min washes three times. The gel was then incubated with secondary antibodies at 4°C overnight, followed by a 30 to 60 min incubation at 37°C before washing in PBS + 0.05% tween 20 as before. The sample was then washed with dH_2O three times and left in dH₂O for ~1 h for full re-expansion before imaging. For long-term storage, the gel was immersed in PBS at 4°C. Tubulin labeling was carried out with a mouse monoclonal anti-acetylated tubulin antibody (T6793-6-11B-1, Sigma-Aldrich, 1:250) and followed by either a goat anti-mouse IgG Cy3 (115-165-166, Jackson ImmunoResearch Labs, 1:400) or a goat antimouse IgG Alexa 488 (A11029, Molecular Probes, 1:400). CEN2 or CEN3 labeling was carried out using rat anti-CEN2 or CEN3 antibodies (1:150 to 1:200; Leung et al., 2017; Munera Lopez et al., 2022), followed by either a goat anti-rat IgG Alexa488 (A-11006, Molecular Probes, 1:750) or a goat anti-rat IgG Cy3 (112-165-167, Jackson ImmunoResearch Labs, 1:400). The antibodies were diluted in 2% BSA in PBS.

Imaging expanded samples

Expanded samples were placed in a MatTek glass-bottom dish. Excess water around the gel was wicked off with filter paper. To maintain humidity in the chamber, wet filter paper strips were plastered against the inner wall of the dish and the dish remained covered throughout imaging. Wide-field image stacks were collected at zincrements of 0.3 µm using a DeltaVision OMX Flex imaging station with a 60x oil immersion lens (NA 1.42) and immersion oil at refractive index 1.520. Images were deconvolved using Softworx (GE Healthcare-Applied Precision) with the point spread function supplied by the manufacturer. Contrast levels were adjusted to optimize the display.

Determination of the expansion ratio

The degree of expansion was determined by measuring the diameter of the conoid at its basal end in images of the tubulin-antibody labeled ExM samples and in SIM images of live parasites expressing eGFP-tubulin. Image stacks containing parasites viewed perpendicular to their long axis were used for measurement. Within each stack, the optical section closest to the center of the conoid, as judged by the presence in the slice of the intra-conoid MTs, was selected. The diameter of the conoid at its widest point, that is, the basal end, was measured using Fiji (Schindelin et al., 2012). Measurements were made on 7 SIM images of live parasites (diameter = $0.31 \mu m \pm 0.01$, mean ± SEM). Measurements on ExM images from three different experiments gave: 1.76 μ m \pm 0.02, n = 34; 1.43 μ m \pm 0.01, n = 24; 1.74 μ m \pm 0.02, n = 41; corresponding to expansion factors of 5.7, 4.6, and 5.6, with a weighted average of 5.4-fold. This is similar to the expansion factors reported in (Gambarotto et al., 2019).

Interestingly, the diameter of daughter conoids was consistently ~10% larger than adult conoids, a small but statistically significant difference (p = 0.0004). It is difficult to measure conoids of daughters in the SIM images, so it is not clear at present whether this difference in size is real or is caused by a difference between adults and daughters in susceptibility to expansion.

Quantification of APR1-mCherry fluorescence in the parasite apex through daughter development

Live cultures (prepared as noted above for 3D-SIM) were imaged using a DeltaVision OMX Flex imaging station (GE Healthcare-Applied Precision). Wide-field image stacks were collected at z-increments of 0.3 µm using a 60x oil immersion lens (NA 1.42) and immersion oil at refractive index 1.520. The same image acquisition parameters (exposure, gain, and laser intensity) were used for all images. Quantification of APR1-mCherry fluorescence was carried out using Fiji (Schindelin et al., 2012), employing raw images. The corrected fluorescence intensity was calculated by subtracting the background (measured on an area adjacent to the apical polar ring) from the total fluorescence (sum of all pixel values in an oval region enclosing the apical polar ring).

ACKNOWLEDGMENTS

We thank Melissa Molina for tissue culture support, Dr. Jonathan Munera Lopez and Ms Isadonna F. Tengganu for helpful discussions. This study was supported by funding from the National Institutes of Health/National Institute of Allergy and Infectious Diseases (R01-Al132463) awarded to K.H. and from the National Science Foundation (2119963) awarded to K.H. (co-PI).

REFERENCES

- Azimzadeh J, Marshall WF (2010). Building the centriole. Curr Biol 20, R816-R825.
- Back PS, O'Shaughnessy WJ, Moon AS, Dewangan PS, Hu X, Sha J, Wohlschlegel JA, Bradley PJ, Reese ML. (2020). Ancient MAPK ERK7 is regulated by an unusual inhibitory scaffold required for Toxoplasma apical complex biogenesis. Proc Natl Acad Sci USA 117, 12164-12173.
- Back PS, O'Shaughnessy WJ, Moon AS, Dewangan PS, Reese ML, Bradley PJ (2021). Multivalent interactions drive the Toxoplasma AC9:AC10:ERK7 complex to concentrate ERK7 in the apical cap. MBio 13, e0286421.
- Bannister LH, Mitchell GH (1995). The role of the cytoskeleton in Plasmodium falciparum merozoite biology: an electron-microscopic view. Ann Trop Med Parasitol 89, 105–111.
- Bettencourt-Dias M (2013). Q&A: Who needs a centrosome? BMC Biol 11, 28. Bounkeua V, Li F, Vinetz JM (2010). In vitro generation of Plasmodium falciparum ookinetes. Am J Trop Med Hyg 83, 1187-1194.
- Checkley W, White AC, Jr., Jaganath D, Arrowood MJ, Chalmers RM, Chen X-M, Fayer R, Griffiths JK, Guerrant RL, Hedstrom L, et al. (2015). A review of the global burden, novel diagnostics, therapeutics, and vaccine targets for cryptosporidium. Lancet Infect Dis 15, 85-94.
- Chen C-T, Gubbels M-J (2013). The Toxoplasma gondii centrosome is the platform for internal daughter budding as revealed by a Nek1 kinase mutant. J Cell Sci 126, 3344-3355.
- Chen F, Tillberg PW, Boyden ES (2015). Optical imaging. Expansion microscopy. Science 347, 543-548.
- Damstra HGJ, Mohar B, Eddison M, Akhmanova A, Kapitein LC, Tillberg PW (2022). Visualizing cellular and tissue ultrastructure using Ten-fold Robust Expansion Microscopy (TREx). eLife 11, e73775.
- Dos Santos Pacheco N, Tosetti N, Krishnan A, Haase R, Maco B, Suarez C, Ren B, Soldati-Favre D. (2021). Revisiting the role of Toxoplasma gondii ERK7 in the maintenance and stability of the apical complex. MBio 12,
- Dubremetz JF, Elsner YY (1979). Ultrastructural study of schizogony of Eimeria bovis in cell cultures. J Protozool 26, 367-376.
- Fennell BJ, Naughton JA, Dempsey E, Bell A (2006). Cellular and molecular actions of dinitroaniline and phosphorothioamidate herbicides on Plasmodium falciparum: tubulin as a specific antimalarial target. Mol Biochem Parasitol 145, 226-238.

- Francia ME, Jordan CN, Patel JD, Sheiner L, Demerly JL, Fellows JD, de Leon JC, Morrissette NS, Dubremetz J-F, Striepen B (2012). Cell division in Apicomplexan parasites is organized by a homolog of the striated rootlet fiber of algal flagella. PLoS Biol 10, e1001444.
- Francia ME, Striepen B (2014). Cell division in apicomplexan parasites. Nat Rev Microbiol 12, 125–136.
- Gambarotto D, Zwettler FU, Le Guennec M, Schmidt-Cernohorska M, Fortun D, Borgers S, Heine J, Schloetel JG, Reuss M, Unser M, et al. (2019). Imaging cellular ultrastructures using expansion microscopy (U-ExM). Nat Methods 16, 71–74.
- Garnham PC, Bird RG, Baker JR (1962). Electron microscope studies of motile stages of malaria parasites. III. The ookinetes of *Haemamoeba* and *Plasmodium*. Trans R Soc Trop Med Hyg 56, 116–120.
- Gui L, O'Shaughnessy WJ, Cai K, Reetz E, Reese ML, Nicastro D. (2023). Cryo-tomography reveals rigid-body motion and organization of apicomplexan invasion machinery. Nat Commun 14, 1775.
- Hepler PK, Huff CG, Sprinz H (1966). The fine structure of the Exoerythrocytic stages of *Plasmodium* fallax. J Cell Biol 30, 333–358.
- Hu K (2008). Organizational changes of the daughter basal complex during the parasite replication of *Toxoplasma gondii*. PLoS Pathogens 4, 108–121.
- Hu K, Johnson J, Florens L, Fraunholz M, Suravajjala S, DiLullo C, Yates J, Roos DS, Murray JM (2006). Cytoskeletal components of an invasion machine – the apical complex of *Toxoplasma gondii*. PloS pathogens 2, 0121–0139.
- Hu K, Mann T, Striepen B, Beckers CJ, Roos DS, Murray JM (2002a). Daughter cell assembly in the protozoan parasite *Toxoplasma gondii*. Mol Biol Cell 13, 593–606.
- Hu K, Roos DS, Murray JM (2002b). A novel polymer of tubulin forms the conoid of *Toxoplasma gondii*. J Cell Biol 156, 1039–1050.
- Janouškovec J, Tikhonenkov DV, Burki F, Howe AT, Kolísko M, Mylnikov AP, Keeling PJ (2015). Factors mediating plastid dependency and the origins of parasitism in apicomplexans and their close relatives. Proc Natl Acad Sci USA 112, 10200–10207.
- Joshi HC (1994). Microtubule organizing centers and gamma-tubulin. Curr Opin Cell Biol 6, 54–62.
- Klimas A, Gallagher BR, Wijesekara P, Fekir S, DiBernardo EF, Cheng Z, Stolz DB, Cambi F, Watkins SC, Brody SL, et al. (2023). Magnify is a universal molecular anchoring strategy for expansion microscopy. Nat Biotechnol 41, 858–869.
- Kollman JM, Zelter A, Muller EG, Fox B, Rice LM, Davis TN, Agard DA (2008). The structure of the gamma-tubulin small complex: implications of its architecture and flexibility for microtubule nucleation. Mol Biol Cell 19, 207–215.
- Leung JM, He Y, Zhang F, Hwang YC, Nagayasu E, Liu J, Murray JM, Hu K (2017). Stability and function of a putative microtubule organizing center in the human parasite *Toxoplasma gondii*. Mol Biol Cell 28, 1361–1378.
- Leung JM, Liu J, Wetzel LA, Hu K (2019). Centrin2 from the human parasite *Toxoplasma gondii* is required for its invasion and intracellular replication. J Cell Sci 132, jcs228791.
- Leung JM, Nagayasu E, Hwang Y-C, Liu J, Pierce PG, Phan IQ, Prentice RA, Murray JM, Hu K (2020). A doublecortin-domain protein of *Toxoplasma* and its orthologues bind to and modify the structure and organization of tubulin polymers. BMC Mol Cell Biol 21, 8.
- Li Z, Du W, Yang J, Lai D-H, Lun Z-R, Guo Q (2023). Cryo-Electron Tomography of *Toxoplasma gondii* indicates that the conoid fiber may be derived from microtubules. Adv Sci (Weinh) 10, 2206595.
- Liffner B, Absalon S. (2023). Expansion microscopy of apicomplexan parasites. Mol Microbiol, https://doi.org/10.1111/mmi.15135.
- Liu J, He Y, Benmerzouga I, Sullivan WJ Jr., Morrissette NS, Murray JM, Hu K. (2015). An ensemble of specifically targeted proteins stabilizes cortical microtubules in the human parasite *Toxoplasma gondii*. Mol Biol Cell 27, 549–571.
- Liu J, Wetzel L, Zhang Y, Nagayasu E, Ems-McClung S, Florens L, Hu K (2013). Novel Thioredoxin-like proteins are components of a protein complex coating the cortical microtubules of *Toxoplasma gondii*. Eukaryot Cell 12, 1588–1599.
- Long S, Anthony B, Drewry LL, Sibley LD (2017). A conserved ankyrin repeat-containing protein regulates conoid stability, motility and cell invasion in *Toxoplasma gondii*. Nat Commun 8, 2236.
- Mitchison TJ (1988). Microtubule dynamics and kinetochore function in mitosis. Annu Rev of Cell Biol 4, 527–549.
- Mitchison TJ (1989). Mitosis: basic concepts. Curr Opin Cell Biol 1, 67–74. Moritz M, Braunfeld MB, Sedat JW, Alberts B, Agard DA (1995). Microtubule nucleation by gamma-tubulin-containing rings in the centrosome. Nature 378, 638–640.

- Morrissette N (2015). Targeting *Toxoplasma* tubules: tubulin, microtubules, and associated proteins in a human pathogen. Eukaryot Cell 14, 2–12.
- Morrissette NS, Murray JM, Roos DS (1997). Subpellicular microtubules associate with an intramembranous particle lattice in the protozoan parasite *Toxoplasma gondii*. J Cell Sci 110, 35–42.
- Morrissette NS, Sibley LD (2002a). Cytoskeleton of apicomplexan parasites. Microbiol Mol Biol Rev 66, 21–38.
- Morrissette NS, Sibley LD (2002b). Disruption of microtubules uncouples budding and nuclear division in *Toxoplasma gondii*. J Cell Sci 115, 1017–1025.
- Munera Lopez J, Tengganu IF, Liu J, Murray JM, Arias Padilla LF, Zhang Y, Brown PT, Florens L, Hu K. (2022). An apical protein, Pcr2, is required for persistent movement by the human parasite *Toxoplasma gondii*. PLoS Pathog 18, e1010776.
- Nagayasu E, Hwang Y-C, Liu J, Murray J, Hu K (2016). Loss of a double-cortin (DCX) domain containing protein causes structural defects in a tubulin-based organelle of *Toxoplasma gondii* and impairs host cell invasion. Mol Biol Cell E16–08–0587
- Nichols BA, Chiappino ML (1987). Cytoskeleton of *Toxoplasma gondii*. J Protozool 34, 217–226.
- O'Shaughnessy WJ, Hu X, Henriquez SA, Reese ML. (2023). *Toxoplasma* ERK7 protects the apical complex from premature degradation. J Cell Biol 222.
- Oakley BR, Paolillo V, Zheng Y (2015). γ-Tubulin complexes in microtubule nucleation and beyond. Mol Biol Cell 26, 2957–2962.
- Oakley CE, Oakley BR (1989). Identification of gamma-tubulin, a new member of the tubulin superfamily encoded by mipA gene of Aspergillus nidulans. Nature 338, 662–664.
- Oborník M, Lukeš J. (2013). Chapter Eight Cell biology of chromerids: Autotrophic relatives to apicomplexan parasites. In: Int Rev Cell Mol Biol, vol. 306, ed. K.W. Jeon: Academic Press, 333–369.
- Patel U, Stearns T (2002). gamma-Tubulin. Curr Biol 12, R408–409.
- Portman N, Foster C, Walker G, Slapeta J (2014). Evidence of intraflagellar transport and apical complex formation in a free-living relative of the apicomplexa. Eukaryot Cell 13, 10–20.
- Qian P, Wang X, Guan C, Fang X, Cai M, Zhong C-qCui Y, Li Y, Yao L, Cui H, et al. (2022). Apical anchorage and stabilization of subpellicular microtubules by apical polar ring ensures *Plasmodium* ookinete infection in mosquito. Nat Commun 13, 7465.
- Roos DS, Donald RG, Morrissette NS, Moulton AL (1994). Molecular tools for genetic dissection of the protozoan parasite *Toxoplasma gondii*. Methods Cell Biol 45, 27–78.
- Russell DG, Burns RG (1984). The polar ring of coccidian sporozoites: A unique microtubule-organizing centre. J Cell Sci 65, 193–207.
- Schindelin J, Arganda-Carreras I, Frise E, Kaynig V, Longair M, Pietzsch T, Preibisch S, Rueden C, Saalfeld S, Schmid B, et al. (2012). Fiji: An open-source platform for biological-image analysis. Nat Methods 9, 474–482
- Seeber F, Steinfelder S (2016). Recent advances in understanding apicomplexan parasites. F1000Res 5, F1000 Faculty Rev-1369.
- Sheffield HG (1970). Schizogony in *Toxoplasma gondii*: an electron microscope study. Proc Helminth Soc Washington 37, 237–242.
- Sheffield HG, Melton ML (1968). The fine structure and reproduction of Toxoplasma gondii. J Parasitol 54, 209–226.
- Stearns T, Evans L, Kirschner M (1991). Gamma-tubulin is a highly conserved component of the centrosome. Cell 65, 825–836.
- Stearns T, Kirschner M (1994). In vitro reconstitution of centrosome assembly and function: The central role of gamma-tubulin. Cell 76, 623–637.
- Stokkermans TJ, Schwartzman JD, Keenan K, Morrissette NS, Tilney LG, Roos DS (1996). Inhibition of *Toxoplasma gondii* replication by dinitroaniline herbicides. Exp Parasitol 84, 355–370.
- Sun SY, Segev-Zarko L[']-A, Chen M, Pintilie GD, Schmid MF, Ludtke SJ, Boothroyd JC, Chiu W (2022). Cryo-ET of *Toxoplasma* parasites gives subnanometer insight into tubulin-based structures. Proc Natl Acad Sci USA 119, e2111661119.
- Suvorova ES, Francia M, Striepen B, White MW (2015). A novel bipartite centrosome coordinates the apicomplexan cell cycle. PLoS Biol 13, e1002093.
- Tengganu IF, Arias Padilla LF, Munera Lopez J, Liu J, Brown PT, Murray JM, Hu K. (2023). The cortical microtubules of *Toxoplasma gondii* underlie the helicity of parasite movement. J Cell Sci 136, jcs261270.
- Torgerson PR, Mastroiacovo P (2013). The global burden of congenital toxoplasmosis: A systematic review. Bull World Health Organ 91, 501–508.
- Tosetti N, Dos Santos Pacheco N, Bertiaux E, Maco B, Bournonville L, Hamel V, Guichard P, Soldati-Favre D. (2020). Essential function of the

- alveolin network in the subpellicular microtubules and conoid assembly in Toxoplasma gondii. eLife 9, e56635.
- Tran JQ, Li C, Chyan A, Chung L, Morrissette NS (2012). SPM1 stabilizes subpellicular microtubules in Toxoplasma gondii. Eukaryot Cell 11, 206-216.
- Vincent L, Romuald H, Olivier M, Marine HL, Dominique S-F, Virginie H, Paul G. (2022). Nanoscopy of organelles and tissues with iterative ultrastructure expansion microscopy (iU-ExM). bioRxiv, https://doi.org/ 10.1101/2022.11.14.516383.
- Voß Y, Klaus S, Guizetti J, Ganter M (2023). Plasmodium schizogony, a chronology of the parasite's cell cycle in the blood stage. PLoS Pathog 19, e1011157.
- Wadsworth P (1993). Mitosis: spindle assembly and chromosome motion. Curr Opin Cell Biol Feb.5., 123-128.
- Wang X, Fu Y, Beatty WL, Ma M, Brown A, Sibley LD, Zhang R (2021). Cryo-EM structure of cortical microtubules from human parasite Toxoplasma gondii identifies their microtubule inner proteins. Nat Commun 12, 3065.
- Wang X, Qian P, Cui H, Yao L, Yuan J (2020). A protein palmitoylation cascade regulates microtubule cytoskeleton integrity in Plasmodium. EMBO J 39, e104168-e104168.
- Wassie AT, Zhao Y, Boyden ES (2019). Expansion microscopy: principles and uses in biological research. Nat Methods 16, 33-41.
- Woo YH, Ansari H, Otto TD, Klinger CM, Kolisko M, Michálek J, Saxena A, Shanmugam D, Tayyrov A, Veluchamy A, et al. (2015). Chromerid genomes reveal the evolutionary path from photosynthetic algae to obligate intracellular parasites. eLife 4, e06974.
- World-Health-Organization (2022). Worlds Malaria Report 2022, 293.